Available online at www.sciencedirect.com
ScienceDirect
Journal of Sound and Vibration 321 (2009) 65–78
JOURNAL OF SOUND AND VIBRATION
www.elsevier.com/locate/jsvi

An energy-balance approach for oscillator parameter identification

B.P. Mann*, F.A. Khasawneh

Department of Mechanical Engineering and Material Science, Duke University, Durham, NC 27708, USA

Received 8 February 2008; received in revised form 7 May 2008; accepted 18 September 2008
Handling Editor: S. Bolton
Available online 7 November 2008

Abstract

An energy-based approach for parametric nonlinear identification was investigated. The presented method uses an energy balance on the oscillator governing equations for identification purposes, thus requiring the availability of the position and velocity signals. Since it is rarely practical to measure every state variable in an experimental setting, we describe an alternative procedure for estimating velocity from the measured displacement. The presented approach uses cubic smoothing splines to avoid the noise amplification effect that occurs for numerical signal derivatives. Finally, we investigate the identification of parameters from both numerical and experimental data for three nonlinear oscillators. These studies demonstrate the effectiveness of the presented energy-balance approach for transient, periodic, and chaotic response behavior.

1. Introduction

The identification of model parameters from measured data is a common challenge for experimentalists. More specifically, the ability to match theoretical predictions with the observed behavior of a particular system is often dependent upon an accurate approach for extracting the system's physical parameters. Thus there exist a growing body of literature on parametric identification methodologies for both linear and nonlinear systems (e.g. see Refs. [1,2]). One interesting observation is that several methodologies have been developed to overcome the limitations of a particular application. For example, a force balance can be applied if the displacement, velocity, and acceleration signals are available [1]. However, this is usually not the case in many experimental settings and the result of using the numerical signal derivatives is a magnification in measurement noise. Another alternative is to directly measure acceleration and then use numerical integration to generate velocity and displacement signals. While this approach provides a viable alternative for some applications, acceleration measurements are contact measurements where an accelerometer is attached to the physical system of interest. This can prove problematic in many systems since adding mass and measurement cables can alter the dynamics of the original system.

*Corresponding author.
E-mail address: brian.mann@duke.edu (B.P. Mann).

0022-460X/$ - see front matter © 2008 Elsevier Ltd. All rights reserved.
doi:10.1016/j.jsv.2008.09.036

In addition to the types of measurements that are available, other considerations, such as the type of response behavior, can also limit the applicability of a parameter identification scheme. As an example, the approach of Ref. [2] can be applied if the response behavior of a system can be classified as a steady-state periodic response. For impulse and transient responses of weakly nonlinear oscillators, the results from Refs. [3,4] are available. However, relatively fewer methods exist that can be applied to general types of response behaviors (e.g. transient, steady-state, or chaotic responses).

Several recent works have investigated the complications of parameter identification from either a chaotic excitation or chaotic response [5–8]. In particular, the work of Refs. [5–7] have extended the harmonic balance method of Ref. [2] to extracted unstable periodic orbits for parametric nonlinear identification. Others, such as Nichols and Virgin [9] and Pecora and Caroll [10] have focused on the use of chaotic excitation.

This paper investigates an energy-balance approach for parametric nonlinear identification. The general idea is to develop a parameter identification approach that can be applied to any type of continuous oscillator response while simultaneously overcoming the inability to measure each state variable. We use cubic smoothing splines on empirical data (i.e. experimental or numerical data) to demonstrate the reliability of the presented approach on three nonlinear oscillators. Experimental and numerical results are first used to investigate parameter identification on the transient response of a prototypical nonlinear system—the planar pendulum. The nonlinearity of the system is then greatly increased by the addition of two magnets which augment the potential energy wells to that of a bistable system. An approximate expression for the magnetic restoring force, one that is based upon the work of Ref. [5], is assumed in the form of a series expansion. Finally, the energy-balance identification approach is investigated for the chaotic response of a Duffing oscillator.

The content from this paper is organized as follows. The next section describes the energy-balance approach using the equations of a forced Duffing oscillator. This section also includes a brief discussion on the implementation of cubic smoothing splines. The third section describes the experimental system that is investigated in the fourth and fifth sections. Parameter identification studies start in the fourth section and compare parametric identification results for a planar pendulum. Comparisons are made between parameter fitting from an approximate analytical solution and the energy-balance approach. The energy-balance nonlinear identification technique is then applied to numerical and experimental magnetic pendulum data before investigating the reliability of the approach for the chaotic response of a forced Duffing oscillator.

2. Energy-balance identification

This section describes the salient features of the energy-balance approach for parameter identification. Since both position and velocity states are required for implementation, the latter part of this section will describe the use of smoothing splines to obtain velocity from the measured displacement. Although the energy-balance approach is quite general and can be applied to many various systems, we have chosen to illustrate the approach by applying it to a Duffing oscillator with viscous damping and harmonic excitation,

$$m\ddot{x} + c\dot{x} + kx + k_3x^3 = F\cos\Omega t, \tag{1}$$

where m is the mass, c is a viscous damping coefficient, k is a linear stiffness coefficient, and k_3 is a nonlinear stiffness coefficient. The harmonic excitation force is characterized by the force amplitude, F, and excitation frequency, Ω. Multiple methods can be used to balance the energy in Eq. (1). For instance, Eq. (1) can be multiplied by $\mathrm{d}x$ and integrated over the motion path, as discussed in Ref. [11], or Eq. (1) can be multiplied by $\dot{x}$ and integrated over time,

$$\int_{t_1}^{t_2}(m\ddot{x} + c\dot{x} + kx + k_3x^3)\dot{x}\,\mathrm{d}t = \int_{t_1}^{t_2}\dot{x}F\cos\Omega t\,\mathrm{d}t, \tag{2}$$

from a start time t_1 to a final time of interest, denoted by t_2. Using integration by parts for the inertia and restoring force terms, the energy balance of Eq. (2) can be written as

$$T_{1\to2} + U_{1\to2} = W_{\mathrm{in}} - W_d, \tag{3}$$

where $T_{1\to2}$ is the change in kinetic energy, $U_{1\to2}$ is the change in potential energy, W_{in} is the added work of the external force, and W_d is the work due to energy dissipation over the time interval from t_1 to t_2. The individual terms of Eq. (3) are given by

$$T_{1\to2} = \tfrac{1}{2}m(\dot{x}(t_2)^2 - \dot{x}(t_1)^2), \tag{4a}$$

$$U_{1\to2} = \tfrac{1}{2}k(x(t_2)^2 - x(t_1)^2) + \tfrac{1}{4}k_3(x(t_2)^4 - x(t_1)^4), \tag{4b}$$

$$W_{\text{in}} = \int_{t_1}^{t_2} \dot{x}F\cos\Omega t\,\mathrm{d}t, \tag{4c}$$

$$W_d = \int_{t_1}^{t_2} c\dot{x}^2\,\mathrm{d}t. \tag{4d}$$

Eqs. (3)–(4d) show that the position, velocity, and excitation force signals are required to make the energy-balance quantitative and useful for parameter identification. Thus it becomes necessary to estimate the velocity when it is not convenient to measure this state variable.

2.1. Data smoothing

It is rarely practical to measure each state variable in an experimental setting. For instance, it was only convenient to measure the angular displacement data for pendulum experiments that follow. Thus it becomes necessary to apply alternative techniques to estimate the unmeasured state variables. While the state variable

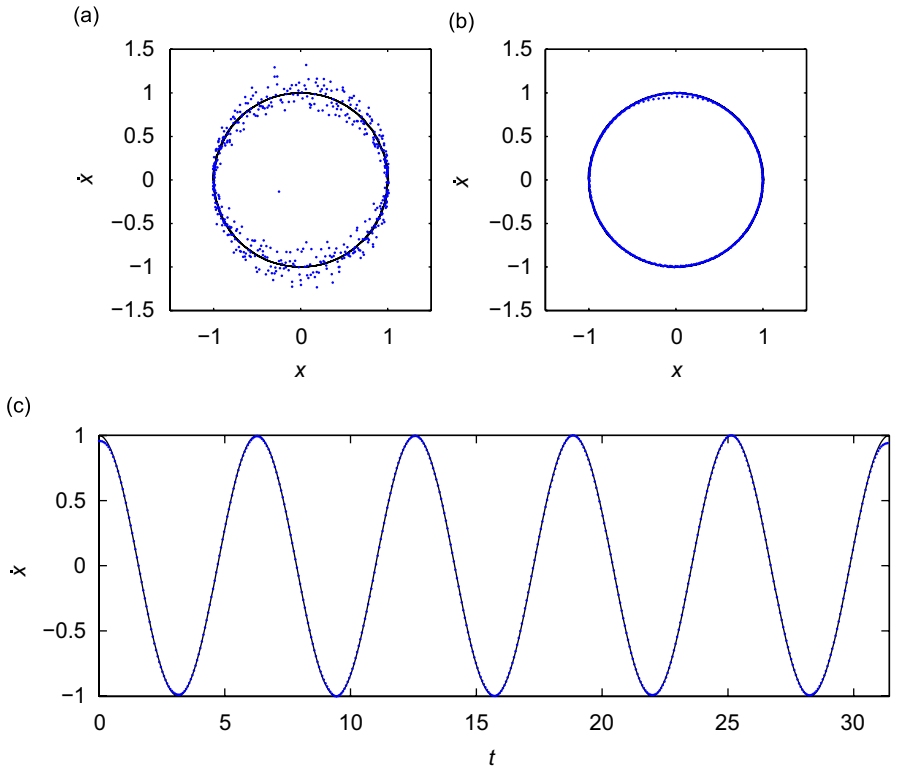

Fig. 1. Comparison of cubic splines with cubic smoothing splines. Graphs (a) and (b) are phase portraits that compare the actual x and $\dot{x}$ to a cubic spline fit (graph (a)) and a cubic smoothing spline fit (graph (b)) once noise has been added. Graph (c) shows $\dot{x}$ plotted against the smoothing spline velocity estimate.

estimation can be accomplished using elements of control theory, such as the Kalman filter [12], we describe an alternative approach that is useful for signals with a moderate amount of noise.

Cubic splines are often applied to empirical data to estimate interim data points or points that lie between two measurements. The basic idea is to fit the data with a piecewise polynomial,

$$x(t) = b_{k0} + b_{k1}(t - t_k) + b_{k2}(t - t_k)^2 + b_{k3}(t - t_k)^3, \tag{5}$$

where the polynomial coefficients b_{k0}, b_{k1}, b_{k2}, and b_{k3} have subscripts that denote their validity between two neighboring data points—the time interval from t_k to t_{k+1}. Therefore, cubic splines provide a piecewise fit to the data while simultaneously giving the desired functional representation for the velocity (i.e. after differentiation of Eq. (5)). Furthermore, cubic splines invoke continuity in the angular displacement, velocity, and acceleration at the intersection with neighboring time steps [13].

Smoothing splines, which are different than the typical spline fitting operation, provide a refinement to the idea using a cubic polynomial to fit empirical data. The basic difference lies in the introduction of a smoothing parameter which reduces noise amplification in the signal derivatives by balancing a fit between the measured data and the smoothness of the second derivative [14]. In the results that follow, cubic smoothing splines have been implemented to avoid noise magnification in estimated velocity, similar to the noise amplification that occurs in a numerical signal derivative, that is caused by the typical spline operation.

Fig. 1 shows a comparison between using smoothing and regular cubic splines to fit a sinusoidal displacement signal. Each of the graphs show the noise free signal, $x = \sin t$, combined with a random noise signal, $0.02\sigma(t)$, where $\sigma(t)$ is random noise with a zero mean and normal distribution. Fig. 1a shows the phase portrait when using regular cubic splines to estimate $\dot{x}$. A noticeable outcome is the magnification in the signal noise from this approach. The phase portrait of Fig. 1b shows the estimate for $\dot{x}$ is nearly identical to the actual velocity when using cubic smoothing splines. This improved velocity estimate and filtering effect is further confirmed by the actual and smoothing spline velocity estimate in the time series of Fig. 1c.

3. Experimental apparatus description

The apparatus described here is used throughout the next two sections to investigate the reliability of the parameter identification approach. A schematic diagram of the experimental system is shown in Fig. 2. Measurements of the pendulum angular oscillations were obtained by supplying a constant voltage to a Novatechnik,[1] model P2200, low-torque potentiometer and recording the time varying voltage drop provided by the potentiometer internal resistor. The potentiometer was housed in a rigid fixture and connected to a ferromagnetic, 75 mm long, threaded rod that was inserted into a 19 mm diameter stainless steel sphere. The mass of the assembled pendulum sphere and rod was measured to be $m = 0.035$ kg. The pendulum base fixture was fabricated from aluminum and rigidly mounted onto a table top. A magnetic potential was created by mounting two neodymium magnets, grade N38, in close proximity to the pendulum rod. A specific feature of the mounting plate was that it was constructed to have pinned locating features. The purpose of the locating features was to provide very repeatable positioning of the magnets which were removed for the parameter identification investigations of Section 4 and replaced to obtain the results of Section 5.

4. Unforced pendulum oscillations

This section describes efforts undertaken to identify the pendulum model parameters. Results are compared for two different nonlinear identification approaches. The first approach fits model parameters to the empirical data using an approximate analytical solution obtained from the method of averaging. This technique is then compared with the energy-balance technique for both relatively small and large amplitude motions. A specific goal is to highlight the effectiveness of these methods for a common experimental case—when only a position coordinate and not the velocity coordinate is measured. Selected results are shown for two types of empirical data: (1) data generated from numerical simulation and (2) data obtained from the experimental system in the absence of the magnets.

[1]Commercial equipment is identified for completeness and does not necessarily imply endorsement by the authors.

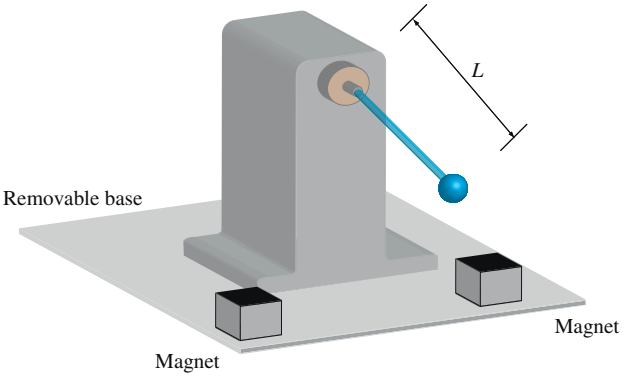

Fig. 2. Schematic diagram of the experimental system with removable magnets to allow for separate characterization of the pendulum and magnetic forces.

4.1. Identification from averaged solution

The governing equation for the unforced oscillations of a planar pendulum with viscous damping is

$$mL^2\ddot{\theta} + c\dot{\theta} + mgL\sin\theta = 0, \tag{6}$$

where θ is the pendulum angular position, c is the damping force constant, $g = 9.81\,\mathrm{m/s^2}$ is the gravitational constant, and L is the pendulum effective length. Here, the term effective length is used in place of the actual pendulum length to denote that the effective length is the distance between the pendulum pivot point and the location of the center of mass. A more convenient form for this equation is

$$\ddot{\theta} + 2\mu\omega\dot{\theta} + \omega^2\sin\theta = 0, \tag{7}$$

where $\mu = c/(mL^2)$ is the damping coefficient and $\omega = \sqrt{g/L}$ is the pendulum natural frequency. The first step for obtaining an approximate analytical solution to Eq. (7) requires an expansion of the sinusoidal term into a Taylor series about the downward position, $\omega^2\sin\theta \approx \omega^2(\theta - \frac{1}{6}\theta^3) = \omega^2\theta + \beta\theta^3$, where $\beta = -\omega^2/6$ and the terms of the order $\mathcal{O}(\theta^5)$ have been truncated from the expansion. After substituting this approximation into Eq. (7), the revised equation of motion can be written as

$$\ddot{\theta} + \omega^2\theta = -f(\theta,\dot{\theta}), \tag{8}$$

where $f(\theta,\dot{\theta}) = 2\mu\omega\dot{\theta} + \beta\theta^3$. Following Ref. [15], the method of averaging is applied by assuming a solution of the form

$$\theta(t) = a\cos(\omega t + \phi) = a\cos\psi, \tag{9}$$

where $\psi = \omega t + \phi$. This will result in the following expressions for the slow variations of a and ϕ

$$\dot{a} = \frac{1}{2\pi\omega}\int_0^{2\pi}\sin\psi f(a\cos\psi, -a\omega\sin\psi)\,\mathrm{d}\psi = -\mu\omega a, \tag{10a}$$

$$\dot{\phi} = \frac{1}{2\pi\omega a}\int_0^{2\pi}\cos\psi f(a\cos\psi, -a\omega\sin\psi)\,\mathrm{d}\psi = \frac{3a^2\beta}{8\omega}. \tag{10b}$$

After substituting $\beta = -\omega^2/6$, the amplitude and phase relationships become

$$a = a_0 e^{-\mu\omega t}, \tag{11a}$$

$$\phi = \frac{a_0^2}{32\zeta}(e^{-2\mu\omega t} - 1) + \phi_0, \tag{11b}$$

where a_0 and ϕ_0 are constants of integration. If the system is started from rest with an initial angular displacement of ϑ_0, the resulting transient solution becomes

$$\theta(t) = \vartheta_0 e^{-\mu\omega t}\cos\left(\omega t + \frac{\vartheta_0^2}{32\mu}(e^{-2\mu\omega t} - 1)\right), \tag{12}$$

which is in agreement with the approximate analytical solution found using the method of multiple scales in Ref. [16]. To solve for the unknown system parameters, the time series from Eq. (12) will be compared with either numerical or experimental data. More specifically, an optimization algorithm is used to estimate the pendulum parameters by fitting the analytical solution to empirical data while minimizing the error in the following cost function:

$$E_T = \sum_{k=1}^{N} (\theta_m(t_k) - \theta(t_k))^2, \tag{13}$$

where N is the total number of data samples and $\theta_m(t_k)$ is the measured value at the kth point in time. The algorithm uses a trust region approach to optimize based on the interior-reflective Newton method [17]. Results from this approach are further described during the comparisons of the next section.

4.2. Energy-based identification comparisons

An energy-based parameter identification scheme is formulated by writing an energy balance between any two arbitrary points in time, t_1 and t_2, as follows:

$$T_{1\to 2} + U_{1\to 2} = -W_d, \tag{14}$$

where $T_{1\to 2}$ is the change in kinetic energy, $U_{1\to 2}$ is the change in potential energy, and W_d is the work due to energy dissipation over the time interval from t_1 to t_2. The terms expressing the energy and work due to dissipation are given by

$$T_{1\to 2} = \tfrac{1}{2}mL^2(\dot\theta^2(t_2) - \dot\theta^2(t_1)), \tag{15a}$$

$$U_{1\to 2} = mL^2\omega^2(\cos\theta(t_1) - \cos\theta(t_2)), \tag{15b}$$

$$W_d = mL^2\int_{t_1}^{t_2} 2\mu\omega\dot\theta^2(t)\,dt, \tag{15c}$$

Eqs. (15a)–(15c) are then divided by $mL^2/2$ and used to populate a matrix equation that describes the energy relationships over any time interval

$$\begin{bmatrix} \int_{t_1}^{t_2}\dot\theta^2\,dt & \cos\theta(t_1) - \cos\theta(t_2) \\ \int_{t_3}^{t_4}\dot\theta^2\,dt & \cos\theta(t_3) - \cos\theta(t_4) \\ \vdots & \vdots \\ \int_{t_{N-1}}^{t_N}\dot\theta^2\,dt & \cos\theta(t_{N-1}) - \cos\theta(t_N) \end{bmatrix} \begin{bmatrix} 4\mu\omega \\ 2\omega^2 \end{bmatrix} = \begin{bmatrix} \dot\theta^2(t_1) - \dot\theta^2(t_2) \\ \dot\theta^2(t_3) - \dot\theta^2(t_4) \\ \vdots \\ \dot\theta^2(t_{N-1}) - \dot\theta^2(t_N) \end{bmatrix}, \tag{16}$$

where t_N is the time at the Nth time step. This yields a linear relationship between the angular velocity, displacement, and system parameters that can be solved in a least-squares sense [18]. For the interested reader, the details for the integration shown in Eq. (15c) are provided in Appendix A.

Fig. 3a shows a comparison between the errors of the energy-based technique and the averaged solution approach. Each method was applied to identify parameters from time series data that was generated from numerical simulation of Eq. (7) for the parameters $\mu = 0.005$ and $\omega = 11.8\,\text{rad/s}$. A zero initial velocity was used for each simulation, but the initial angular position was incremented to study the influence of the start angle on the identification process. Prior to the identification process, normally distributed random noise with a zero mean and scaled maximum amplitude of $\pi/180$ was added to the angular oscillation data. The error from the identification process was quantified with an

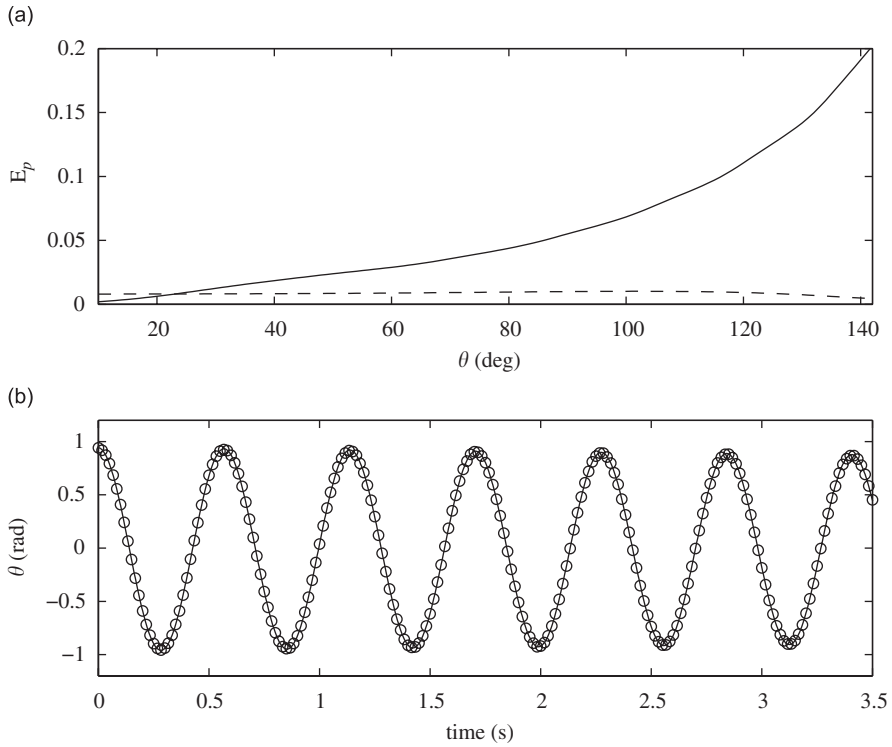

Fig. 3. Graph (a) shows a comparison of errors from the averaged solution (solid line) and the energy-based identification (dashed line). Graph (b) compares the experimentally recorded time series (solid line) and the numerically generated times series (marked with a ○) for the parameters identified with the energy-based approach.

error norm,

$$E_p = \sqrt{\frac{1}{n_p}\left(\left(\frac{\mu_e - \mu}{\mu}\right)^2 + \left(\frac{\omega_e - \omega}{\omega}\right)^2\right)}, \tag{17}$$

where $n_p = 2$ is the number of parameters in the identification process, μ_e is the estimated damping ratio, and ω_e is the estimated natural frequency. Some important conclusion from Fig. 3a are: (1) the error from each method is relatively low for small start angles; (2) the energy-based method provides superior results for relatively larger start angles. While the increase in the parameter identification error from the averaged solution is attributed to the truncation of the higher order nonlinear terms, this also highlights a specific advantage of the energy-balance approach (i.e. it is not necessary to match the solution approximation with the oscillation amplitude).

The energy-balance identification approach was then applied to experimental data from 12 independent free-fall oscillation tests. The tests were anti-alias filtered at 20 Hz with a Stanford Research Systems, model SR640, low-pass filter and recorded at a sample rate of 300 Hz for 10 s time intervals. Using various different start angles, the estimated parameters were averaged over the total number of records to minimize the influence of experimental noise. Fig. 3b shows a comparison time series for the fitted parameters and the measured experimental test. It is noted that the experimental and theoretical results are in good agreement for the estimated pendulum parameters $\omega = 11.74\,\mathrm{rad/s}$ and $\mu = 0.0012$.

5. Unforced magnetic pendulum characterization

This section implements the energy-based identification approach after adding two neodymium magnets to the pendulum system. The result is a highly nonlinear system with magnetic restoration forces that create

Table 1
Unforced magnetic pendulum parameters

Parameter	μ	ω (rad/s)	α_1 (N/rad)	α_2 (N/rad^2)	α_3 (N/rad^3)
Reference	0.0509	11.74	−138.3	21.3	163.1
Estimated	0.0510	11.71	−137.3	21.3	162.9
Experiment	0.0287	11.74	−145.25	25.74	188.11

multiple stable equilibria. The governing equation for the magnetic pendulum is

$$\ddot{\theta} + 2\mu\omega\dot{\theta} + \omega^2 \sin\theta + \sum_{n=1}^{3} \hat{\alpha}_n (n+1)\theta^n = 0\,, \tag{18}$$

where $\hat{\alpha}_n = \alpha_n/mL^2$ and each α_n coefficient describes the magnetic restoring force. The energy-balance expressions between the times t_1 and t_2 are

$$T_{12} = \tfrac{1}{2}mL^2(\dot{\theta}^2(t_2) - \dot{\theta}^2(t_1)), \tag{19a}$$

$$U_{12} = mL^2\left[\omega^2(\cos\theta(t_1) - \cos\theta(t_2)) + \sum_{n=1}^{3} \hat{\alpha}_n(\theta(t_2)^{n+1} - \theta(t_1)^{n+1})\right], \tag{19b}$$

$$W_d = mL^2 \int_{t_1}^{t_2} 2\mu\omega\dot{\theta}^2 \,\mathrm{d}t. \tag{19c}$$

Following the same procedure as in Section 4.2, Eqs. (19a)–(19c) are divided by $mL^2/2$ and arranged into matrix form, $\mathbf{BC} = \mathbf{D}$, with rows that express the energy-balance relationships over a given time interval. The parameters to be identified are contained within the vector $\mathbf{C} = [4\mu\omega\ 2\omega^2\ 2\hat{\alpha}_1\ 2\hat{\alpha}_2\ 2\hat{\alpha}_3]$.

The validity of the above approach was first investigated with numerical simulation prior to experimental implementation. Time series data were generated from numerical simulations of Eq. (18) for the reference parameters listed in Table 1. Prior to the identification process, normally distributed random noise, scaled to have a maximum amplitude of $\pi/180$, was added to the angular oscillation data. To quantify the accuracy of the identified parameters, the following error norm was implemented

$$E_p = \sqrt{\frac{1}{n_p}\left(\left(\frac{\mu_e - \mu}{\mu}\right)^2 + \left(\frac{\omega_e - \omega}{\omega}\right)^2 + \sum_{n=1}^{3}\left(\frac{\alpha_{ne} - \alpha_n}{\alpha_n}\right)^2\right)}, \tag{20}$$

where the number of parameters was set to five, $n_p = 5$, and α_{ne} represents the estimated value of α_n. Fig. 4 shows example phase portraits generated with numerical simulation for both the reference parameters and estimated parameters using four sets of initial conditions. The outcome of the numerical studies, which showed error norm results of $E_p = 0.0037$ or less for numerous initial conditions, demonstrates the goodness of fit in the identification algorithm.

5.1. Application to experimental data

The procedure for experimental trials consisted of orienting the pendulum to an initial start angle and then releasing it from the rest position. During the experimental trials, it was observed that the final pendulum equilibrium position was strongly dependent upon subtle changes in the initial conditions—a hallmark of nonlinear systems. For illustration purposes, two sample results are shown in graphs (a) and (b) of Fig. 5.

The energy-balance identification procedure was applied to 12 experimental trials. A list of the identified model parameters from the experiments is given in Table 1. One parameter of particular interest is the damping ratio, $\mu = 0.0287$, which captures the rate dependent forces for the entire system. The damping ratio

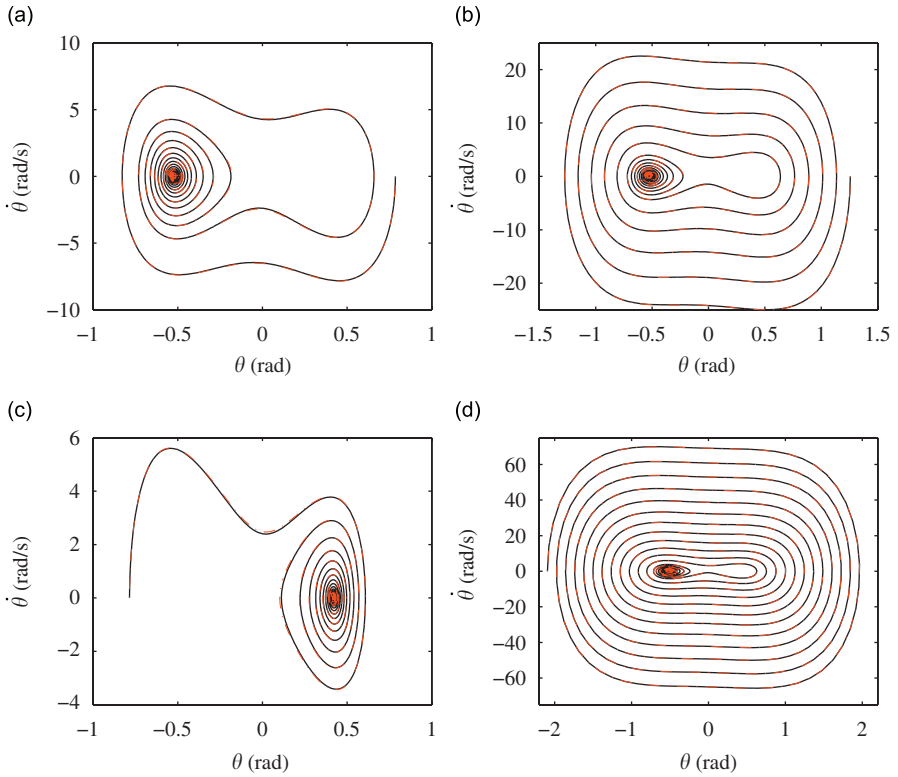

Fig. 4. Comparisons of the simulated phase plane trajectories for the reference parameter set (solid black line) and the estimated parameters obtained from the identification algorithm (dashed grey line). The initial conditions applied to each case are: (a) $\theta(0)=\pi/4$ rad, $\dot{\theta}(0)=0$ rad/s; (b) $\theta(0)=0.4\pi$ rad, $\dot{\theta}(0)=0$ rad/s; (c) $\theta(0)=-\pi/4$ rad, $\dot{\theta}(0)=0$ rad/s; and (d) $\theta(0)=-2/3\pi$ rad, $\dot{\theta}(0)=0$ rad/s.

in the presence of the magnets is shown to greatly increase the energy dissipation of the system. Upon further investigation, the authors recognized the additional rate dependent forces as current damping and/or the result of Faraday's Law (i.e. force is proportional to the time rate of change in the magnetic field) [19].

Graphs (c) and (d) of Fig. 5 provide the comparable numerical time series for the experimental time series of graphs (a) and (b), respectively. These plots were generated by simulating Eq. (18) for the experimental parameters of Table 1. Qualitatively speaking, these two examples yield comparable behavior near the middle of the time series. However, two distinct differences are worthy of mention. The numerical results show a shorter oscillation period for larger oscillation amplitudes than those of the experiment. This discrepancy reverses for small amplitude oscillations with the experimental time series showing a shorter oscillation period. The authors believe the aforementioned differences were due to neglecting the higher order nonlinear terms. Thus our choice to simplify the math model, through the use of fewer magnetic-restoring force coefficients, has resulted in coefficients that show quantitatively different results for the extreme cases—either relatively large or small oscillation amplitudes. Furthermore, it is speculated that nonlinear damping effects could have also contributed [20].

The identified system parameters were also used to construct a one-dimensional basin of attraction to investigate the experimental observation of a strong sensitivity to initial conditions (see Fig. 6a). When comparing the regions of initial conditions that share the same final equilibrium condition, it is intuitive to also view the scaled potential energy well, defined by

$$\frac{U}{mL^2}=\omega^2(1-\cos\theta)+\sum_{n=1}^{3}\hat{\alpha}_n\theta^{n+1}. \tag{21}$$

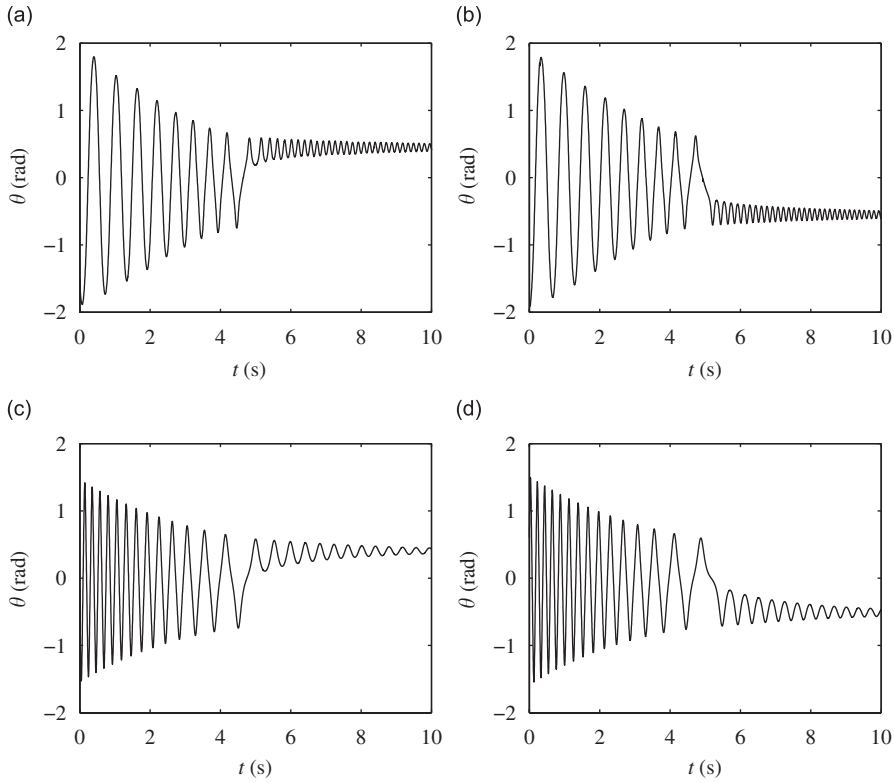

Fig. 5. Time histories are shown for two experimental trials in graphs (a) and (b). Graphs (c) and (d) show numerical simulation data for approximately the same initial conditions as graphs (a) and (b), respectively.

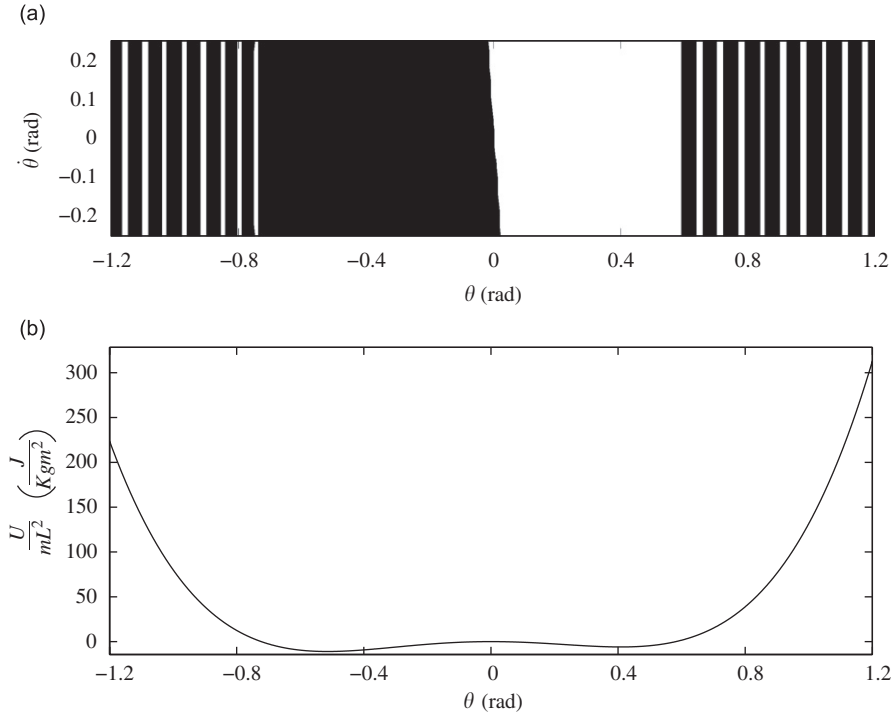

Fig. 6. The numerically generated basins of attraction are shown in graph (a) to illustrate the strong sensitivity to initial conditions. Graph (b) shows the experimentally identified potential energy well divided by the moment of inertia.

In particular, it is interesting to note that initial conditions originating close to an equilibrium position will remain trapped within the same potential well. However, initial conditions that originate further away from a stable equilibrium can overcome the center potential barrier and spill over into the neighboring energy well.

6. Forced response of a Duffing oscillator

While the previous sections have investigated unforced systems, the current section applies the energy-balance approach to the forced Duffing oscillator of Eqs. (1)–(4d). In contrast to the energy-balance approach of Ref. [11], which assumes a periodic oscillator response, we show the current parameter identification scheme can be applied to generic types of response behavior of continuous nonlinear systems (e.g. motions that are periodic, quasi-periodic, and chaotic).

To calculate the work from the harmonic excitation force, as given by Eq. (4c), an analytical expression for the oscillator velocity is required. Combining the derivative of Eq. (5) and the smoothing spline coefficients obtained from fitting the empirical data, the work into the system can be obtained from

$$W_{\text{in}} = \int_{t_k}^{t} \dot{x}(t,t_k) F \cos \Omega t \, \mathrm{d}t = F \sum_{k=1}^{N} [(\gamma_k \cos \Omega t + \eta_k \sin \Omega t)|_{t_k}^{t_{k+1}}], \tag{22}$$

where $\dot{x}(t,t_k)$ is used to describe the estimated velocity from time t_k to time t and N time steps are assumed between t_k and the time of interest, t. The coefficients of Eq. (22) change for each time step and are given by

$$\gamma_k = \frac{2}{\Omega^2}(b_{k2} + 3b_{k3}t - 3b_{k3}t_k), \tag{23a}$$

$$\eta_k = \frac{1}{\Omega}\left(3b_{k3}t_k^2 - 2(b_{k2} + 3b_{k3})t_k + b_{k1} + 2b_{k2} + 3b_{k3}\left(t^2 - \frac{2}{\Omega^2}\right)\right). \tag{23b}$$

Empirical data were obtained by simulating Eq. (1) for the reference parameters of Table 2. This resulted in a chaotic response of the system, see Fig. 7a, which was used for parameter identification after random noise was added. The noise was normally distributed random noise with a zero mean and a scaled maximum amplitude of 1% of the maximum simulated displacement. Parameters were determined by arranging Eqs. (4a)–(4d) into a matrix equation that was solved in a least-squares sense. The error from the parameter identification process was quantified with the following error norm:

$$E_p = \sqrt{\frac{1}{n_p}\left(\left(\frac{m_e - m}{m}\right)^2 + \left(\frac{c_e - c}{c}\right)^2 + \left(\frac{k_e - k}{k}\right)^2 + \left(\frac{k_{3e} - k_3}{k_3}\right)^2\right)}, \tag{24}$$

where m_e is the estimated value of m, c_e is the estimated value of c, k_e is the estimated value of k, k_{3e} is the estimated value of k_3, and the number of parameters was set to four, $n_p = 4$. The estimated parameters, which have been listed in Table 2, resulted in an error norm of $E_p = 0.009$ thus demonstrating the reliability of the presented energy-balance approach. Another consideration is which points to include in the energy balance. For the presented results, we have chosen points spaced 10 forcing periods away to allow the oscillation behavior enough time to morph away from the periodic motion.

Fig. 7 shows phase portraits generated from numerical simulations of the forced Duffing oscillator. Graph (a) used the reference parameters and graph (b) the identified parameters listed in Table 2. Phase plane trajectories are shown for 100 forcing periods that were taken from the steady-state regions of the time series.

Table 2
Forced Duffing oscillator

Parameter	m (kg)	c (N m/s)	k (N/m)	k_3 (N/m^3)
Reference	1	0.2	1	1
Estimated	1.012	0.200	1.013	0.995

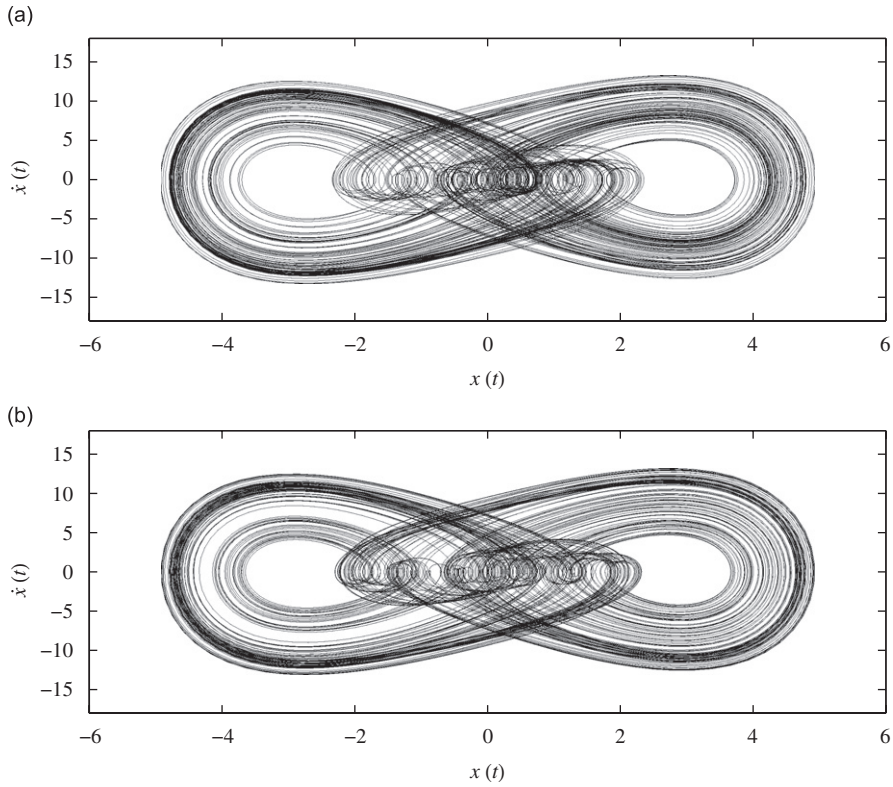

Fig. 7. Phase portraits generated from numerical simulations of the forced Duffing oscillator. Graph (a) used the reference parameters and graph (b) the identified parameters listed in Table 2. Both graphs used $F = 27$ and $\Omega = 1.33$.

Fig. 8 shows the corresponding Poincaré sections for the reference and estimated parameters of Table 2. The results shown in these graphs were simulated over 10,000 oscillation periods. The similarities in both the phase portraits and Poincaré sections are shown to further illustrate the accuracy of the parameter identification scheme.

7. Summary and conclusions

An energy-based approach for parametric nonlinear identification was investigated. Under the assumption that it is rarely practical to measure every state variable in an experimental setting, the velocity state is estimated by fitting the measured displacement data with cubic smoothing splines. Unlike using a signal derivative or regular splines, which can cause noise amplification, smoothing splines are particularly useful because they can mitigate the influence of measurement noise while also providing a polynomial expression for the energy-balance integrations.

Experimental and numerical results were used to investigate parameter identification on the unforced response of a planar pendulum and a magnetic pendulum. For these transient responses, the energy-balance approach is shown to have a specific advantage. This was highlighted in the planar pendulum example which showed the energy-balance technique alleviates the need to match the order of the approximate solution with the oscillation amplitude. The final section investigates the reliability of the energy-balance approach for the forced oscillations of a Duffing oscillator. Parameters are chosen to cause a chaotic response that is used for parameter identification.

In summary, the combination of using an energy-balance energy with cubic smoothing splines was shown to be an effective method for parametric nonlinear identification. Moreover, the presented approach demonstrates the reliability of an energy-balance approach for a broad range of oscillator responses that

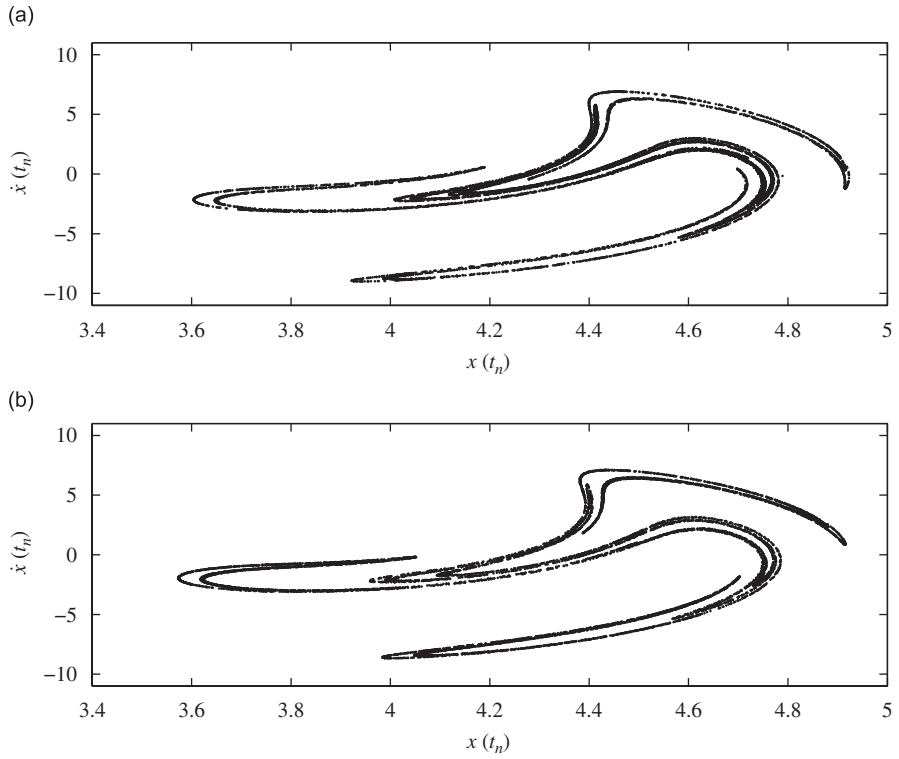

Fig. 8. Poincaré sections generated from numerical simulations of the forced Duffing oscillator. Graph (a) used the reference parameters and graph (b) the identified parameters listed in Table 2. Both graphs used $F = 27$ and $\Omega = 1.33$.

include transient, periodic, and chaotic behavior. A specific limitation for the presented work arises for dynamical systems with non-smooth state variables (e.g. impact oscillators). For such systems, the use of smoothing splines is perhaps inappropriate since any abrupt changes in the state variables will be smoothed.

A possible future extension of the presented work would be to fit the excitation force with splines. Thus the harmonic excitation term, $F\cos\Omega t$, that appears in Eq. (4c) could then be replaced with a piecewise spline polynomial. This would allow more complicated input waveforms, such as chaotic and multifrequency excitations, to be written in the same form and used in the present parameter identification framework.

Acknowledgment

Support from U.S. National Science Foundation CAREER Award (CMS-0636641) is gratefully acknowledged.

Appendix A

When using cubic smoothing splines, the polynomial coefficients are obtained by fitting the empirical data with a cubic polynomial. The polynomial coefficients and the derivative of Eq. (5) can then be used to estimate the velocity,

$$\dot{x}(t,t_k) \approx b_{k1} + 2b_{k2}(t-t_k) + 3b_{k3}(t-t_k)^2, \tag{A.1}$$

for the time interval $t_k \leqslant t \leqslant t_{k+1}$. Eq. (A.1) can then be inserted into the energy dissipation equation

$$W_d = \int_{t_1}^{t_1+\tau} c\dot{x}(t,t_k)^2 = c\sum_{k=1}^{N-1}[(d_k t^5 + e_k t^4 + f_k t^3 + g_k t^2 + h_k t)|_{t_k}^{t_{k+1}}], \tag{A.2}$$

to ascertain the influence of the viscous damping term. The coefficients in this expression are

$$d_k = \frac{9b_{k3}}{5}, \tag{A.3a}$$

$$e_k = 3b_{k3}(b_{k2} - 3b_{k3}t_k), \tag{A.3b}$$

$$f_k = 2(b_{k1}b_{k3} + \tfrac{2}{3}b_{k2}^2 - 6b_{k2}b_{k3}t_k + 9b_{k3}^2t_k^2), \tag{A.3c}$$

$$g_k = 2[b_{k1}b_{k2} - (2b_{k2}^2 + 3b_{k3}b_{k1})t_k + 9b_{k3}b_{k2}t_k^2 - 9b_{k3}^2t_k^3], \tag{A.3d}$$

$$h_k = 9b_{k3}^2t_k^4 - 12b_{k3}b_{k2}t_k^3 + (6b_{k3}b_{k1} + 4b_{k2}^2)t_k^2 - 4b_{k2}b_{k1}t_k + b_{k1}^2. \tag{A.3e}$$

References

[1] K.S. Mohammad, K. Worden, G.R. Tomlinson, Direct parameter estimation for linear and nonlinear structures, *Journal of Sound and Vibration* 152 (3) (1992) 471–499.

[2] K. Yashuda, S. Kawamura, K. Watanabe, Identification of nonlinear multi-degree-of-freedom systems (presentation of an identification technique), *JSME International Journal* 31 (1988) 8–14.

[3] G. Kerschen, V. Lenaerts, J.C. Golinval, Identification of a continuous structure with a geometrical non-linearity. Part 1: conditioned reversed path method, *Journal of Sound and Vibration* 262 (4) (2003) 889–906.

[4] M. Feldman, Non-linear free vibration identification via the Hilbert transform, *Journal of Sound and Vibration* 208 (3) (1997) 475–489.

[5] B.F. Feeny, C.M. Yuan, J.P. Cusmano, Parametric identification of an experimental magneto-elastic oscillator, *Journal of Sound and Vibration* 247 (5) (2001) 785–806.

[6] C.M. Yuan, B.F. Feeny, Parametric identification of chaotic systems, *Journal of Vibration and Control* 4 (4) (1998) 405–426.

[7] Y. Liang, B.F. Feeny, Parametric identification of a based-excited pendulum, *Nonlinear Dynamics* 46 (2006) 17–29.

[8] M.D. Narayanan, S. Narayanan, C. Padmanabhan, Parametric identification of nonlinear systems using chaotic excitation, *Journal of Computational and Nonlinear Dynamics* 2 (2007) 225–231.

[9] J.M. Nichols, L.N. Virgin, System identification through chaotic interrogation, *Mechanical Systems and Signal Processing* 17 (4) (2003) 871–881.

[10] L.M. Pecora, T.L. Caroll, Driving systems with chaotic signals, *Physical Review A* 44 (4) (1991) 2374–2383.

[11] J.W. Liang, B.F. Feeny, Balancing energy to estimate damping parameters in forced oscillators, *Journal of Sound and Vibration* 295 (2006) 988–998.

[12] W.L. Brogran, *Modern Control Theory*, third ed., Prentice-Hall, Upper Saddle River, NJ, 1991.

[13] E. Kreyszig, *Advanced Engineering Mathematics*, eighth ed., Wiley, New York, NY, 1999.

[14] C.D. Boor, *A Practical Guide to Splines*, Springer, New York, NY, 1978.

[15] A.H. Nayfeh, D.T. Mook, *Nonlinear Oscillations*, Wiley, New York, 1979.

[16] B.P. Mann, M.A. Koplow, Symmetry breaking bifurcations of a parametrically excited pendulum, *Nonlinear Dynamics* 46 (4) (2006) 427–437.

[17] T. Coleman, Y. Li, An interior trust region approach for nonlinear minimization subject to bounds, *SIAM Journal on Optimizations* 6 (1996) 418–445.

[18] L.N. Virgin, *Introduction to Experimental Nonlinear Dynamics*, Cambridge University Press, Cambridge, UK, 2000.

[19] D. Haliday, R. Resnick, *Fundamentals of Physics*, third ed., Wiley, New York, NY, 1988.

[20] S. Roundy, P.K. Wright, J.M. Rabaey, *Energy Scavenging for Wireless Sensor Networks*, Springer, New York, 2003.